CAAP Quarterly Report

Date of Report: < *April* 10th, 2018>

Contract Number: <DTPH56-15-H-CAAP06>

Prepared for: <Government Agency: U. S. DOT PHMSA >

Project Title: <*Mitigating Pipeline Corrosion Using A Smart Thermal Spraying Coating System*>

Prepared by: <North Dakota State University>

Contact Information: <Dr. Fardad Azarmi, Email: fardad.azarmi@ndsu.edu, Phone: 701.231.9784; Dr. Ying Huang, Email: ying.huang@ndsu.edu, Phone: 701.231.7651.>

For quarterly period ending: < *April* 10th, 2018>

Business and Activity Section

(a) Generated Commitments

No changes to the existing agreement.

No equipment purchased over this reporting period.

No supplies purchased in this quarter.

(b) Status Update of Past Quarter Activities

In this quarter, studies were mainly focused on the risk management planning capability of utilizing corrosion monitoring system, preparing the full size pipe laboratory test, and finite element analysis (FEA). The new input of FEA study employed an image based FEA method to predict thermomechanical or electrochemical properties of the coating structure. It is a new development in the field of coating materials since experimental measurement of their properties will be a difficult task due to small thickness of the deposited coating (micro millimeter scale). This quarter report started with analyzing mechanical properties of Al-15Zn coating and we will continue with estimation of other properties such as corrosion resistance in future. Further efforts will be focused on continuing analyzing using FEA and the full size pipe experiments, and performing the data collecting and data analysis. The detail progresses, which were completed in this quarter, are presented below:

1) Pipeline Risk Management Planning (Subtask 3.3)

As described in the last quarterly report, the most widely applied risk management framework is the relative risk rating with scoring table model. Our main focus of integrating the corrosion monitoring system into this scoring table is the corrosion part of the model, in which the coating condition weighted 15 points out of 100 points. There are four level of coating conditions defined in the model: 1) good, 2) fair, 3) poor, and 4) absence; and each level grants a score of 15 points, 10 points, 5 points, and 0 point, respectively. However, with a data driven corrosion monitoring system that could monitor the coating condition, the score could be granted continuously from 0 to 15 points without given certain levels, as 0 point for no coating and 15 for good coating condition control.

With the corrosion monitoring system, for any given time noted as t_i, the corrosion rate (noted as r_i) at time t_i is known. So the total corroded depth (noted as D_t) in time t could be shown as follow:

$$D_t = \int_0^t r_i dt$$

In coating design, the original coating thickness (noted as D_o) is known. So the coating condition score (S_{cc}) in the model could be determined as:

$$S_{cc} = \frac{(D_o - D_t)}{D_o} \times 15 = 15 \cdot (1 - \int_0^t \frac{r_i}{D_o} dt) = 15 \cdot (1 - \int_0^t p_i dt)$$

where $p_i = r_i / D_o$ stands for the percentage corrosion rate to the original coating thickness. When applying the corrosion monitoring system on site, with collected corrosion rate data (r_i), the percentage corrosion rate (p_i) could be updated time to time, and the coating condition score could be updated in real-time basis. Pipeline operators could see the score dropping from 15 points as the coating being corroded. When pipes got further corroded and the pipeline's overall relative risk rating increased to a certain value, the pipeline operator may choose to take certain action to counter the potential failure, such as renew the coating.

2) Full size pipe laboratory test preparation (Subtask 4.1)

To validate the capability of proposed corrosion monitoring system, full-size laboratory tests will be set up next quarter. The pipes used in the test are NPS 6 SCH 40 pipes of 10 inches length, shown in **Figure 1**.

(a) (b) (c)

Figure 1. Physical dimensions of the pipes used for future test.

Three types of soil with different compositions and different moisture contents of 20% (Group 1), 30% (Group 2), and 50% (Group 3) will be used to simulate dry, medium, and wet soil condition. The soil samples will be prepared following the U.S. EPA standard 68-C4-0022. In each group of soil, two pipes sections will be buried.

On each pipe, there are four FBG sensors embedded inside the coatings as shown in the Figure 2. Each FBG sensor is capable of detecting corrosion, and with four FBG sensors, the corrosion will be able to be localized. For each pipe, the exact FBG sensor placing location would be slightly different due to the FBG sensor packaging using the stainless steel tubes. However, all location of the FBG sensors were precisely measured for each pipe in order to accomplish corrosion localization goal. Soft coating would be applied when the FBG sensors were all attached to the pipes with mold, and then buried to begin the test during next quarter.

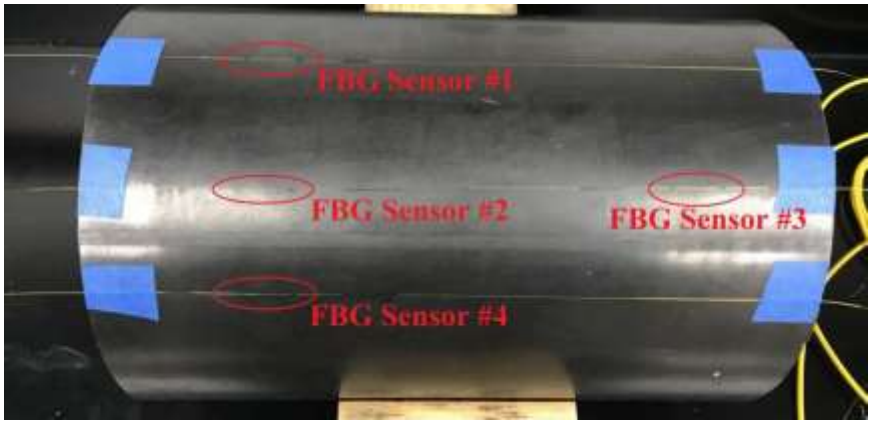

Figure 2. Pipe with FBG sensors installed and ready for deposition of coating.

3) Image based Finite Element Analysis (FEA) (Subtask 2.5 to 2.7)

As it was mentioned in previous reports, it is planned to use an effective method to better understand thermos-mechanical and physical properties of coating structures. Due to the dependency of the mechanical, physical, and electrochemical properties of coatings on microstructural features such as pores, voids, and splat boundaries, it is important to account for these features in finite element models of coating behavior. A schematic of the microstructure of a wire arc sprayed Al-15Zn coating is shown in Figure 3. The Object Oriented Finite (OOF) element analysis program, developed at the Center for Computational and Theoretical Materials Science (CTCMS) at US National Institute of Standards and Technology (NIST), enables complex two dimensional microstructures to be modeled using images of the actual microstructures. This analysis technique has been employed extensively to numerically simulate mechanical and thermophysical properties of coatings and composite materials in recent years [1-2]. Version 2.1.14 of OOF was used for image based numerical simulation in this study.

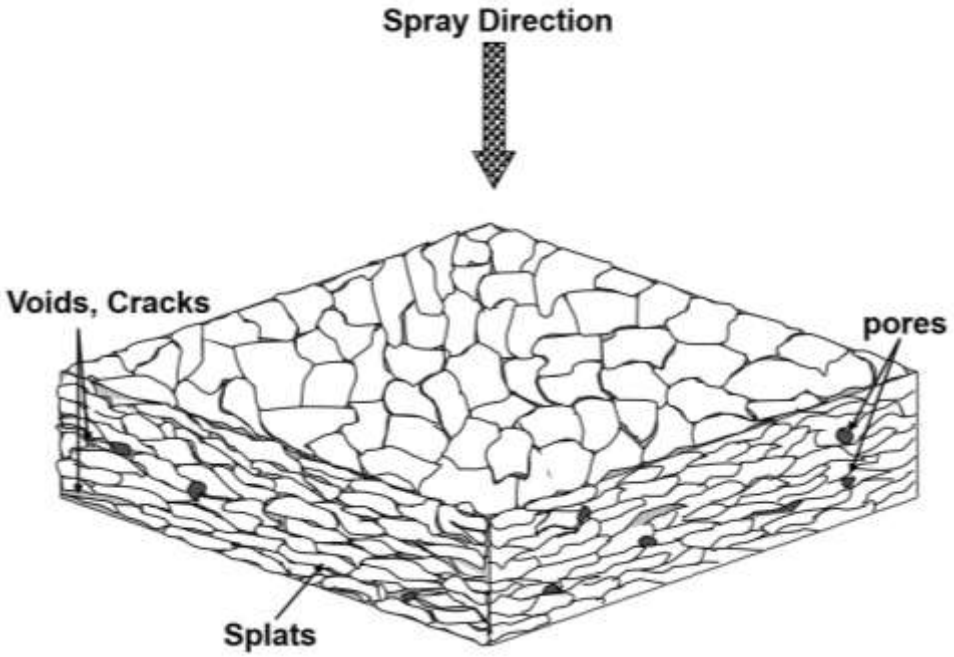

Figure 3. Schematic of microstructure of a Wire Arc sprayed Al-Zn coating.

Image Analysis FEA Process using OOF Software: In the first step several micrographs were taken from randomly selected positions along the polished cross-section of the wire arc sprayed Al-15Zn coatings. Figure 4 shows an optical micrograph of the cross-section of the as-sprayed coating. Next, two groups of pixels were created; Matrix and Pores based on the two different contrasts seen on the microstructure. Dark pixels on the image represent voids and porosities on the coating, while gray ones show the coating material Al-15Zn.

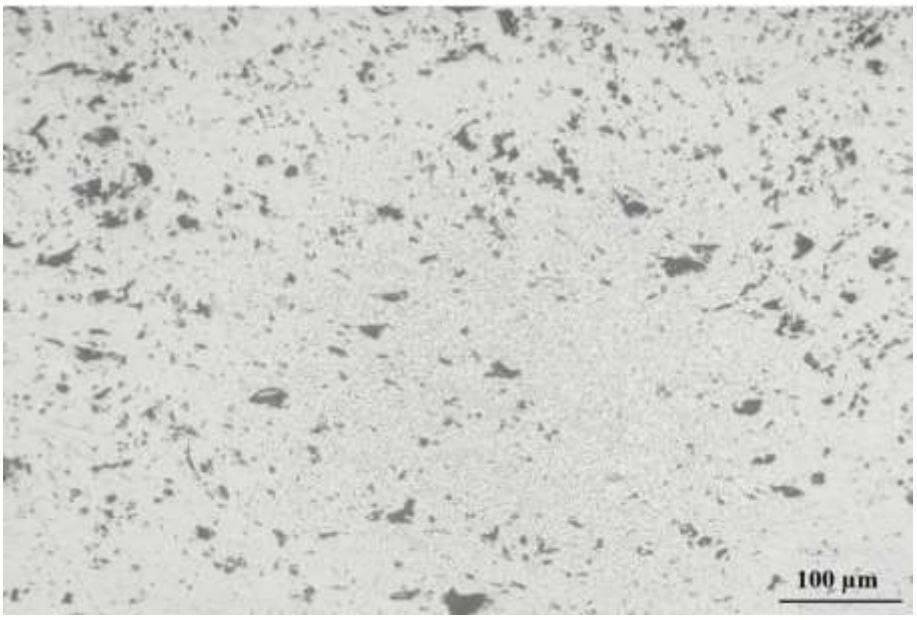

Figure 4. Optical microscopic image of Al-15Zn coating cross-section.

Then, from the graphics window and by choosing Pixel Selection option from toolbox menu, we could select pixels by color difference using RGB method. For this microstructure, a range of 0.2 color difference was suitable to distinguish pores and matrix pixels and assign them to their corresponding groups. In materials menu, elasticity property of each group was created by determining the values for E and ν, which for the matrix were 80 and 0.32, while for the pores they were defined as $1\times e^{-09}$ and 0.32. For voids and pores, we can assume that the Poisson ratio is similar to the value for the matrix to avoid any incompatibility in the software, while the elastic modulus is set to a very small number since it cannot be set to zero. The elastic modulus for pure aluminum is around 70 GPa and it increases by adding zinc to aluminum, as for Al-6Zn it has reported to be around 73 GPa and for Al-9Zn the elastic modulus increased to 77 GPa. The elastic modulus of 80 GPa for the alloy Al-15Zn was selected according to this assumption. Figure 5 shows the processed image after dividing features to two different types of pixels. Assigned properties used for calculation by OOF are listed in Table 1.

Table 1. Mechanical properties of the wire arc Al-15Zn coating

Group	*Elastic Young's Modulus (GPa)*	*Poisson Ratio*
Matrix (Al-15Zn)	80	0.32
Pores (voids)	1e-09	0.32

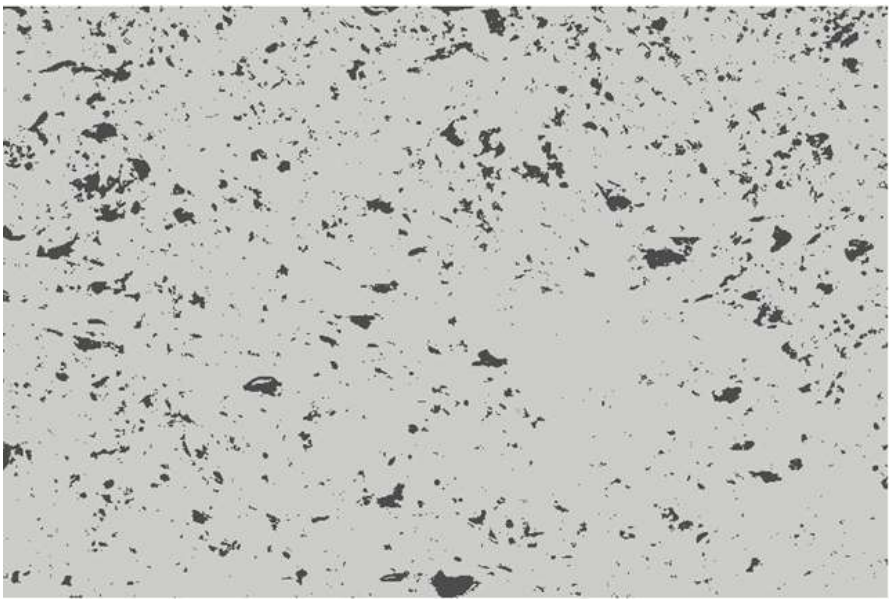

Figure 5. Modified image, Dark and gray pixels representing voids and matrix respectively.

In the next step, elements were defined on the processed image which resulted in creation of a structure which can be meshed for numerical solution. A skeleton structure was created on the micrograph with 210 x-elements and 140 y-elements. This skeleton was modified to increase the homogeneity of elements. It was performed by using different tools such as smooth, snap anneal, snap refine, to increase the smoothness of skeleton. It could produce 120,916 nodes, and total of 204,680 elements including 168,462 triangles and 36,218 quads ones with the homogeneity factor of 0.9886. The skeleton was meshed according the above mentioned condition. The final status of the produced skeleton is shown in the Table 2.

Table 2. Skeleton status created and modified by OOF.

Number of nodes	*Number of elements*	*Triangle elements*	*Quadratic elements*	*Homogeneity index*
120916	204680	168462	36218	0.9886

Figure 6 shows the meshed image ready for application of force or stress. The distribution of elements around different microstructural features are shown in inset image in this figure. As mentioned before, the accuracy of the simulation will be greatly improved by annealing process.

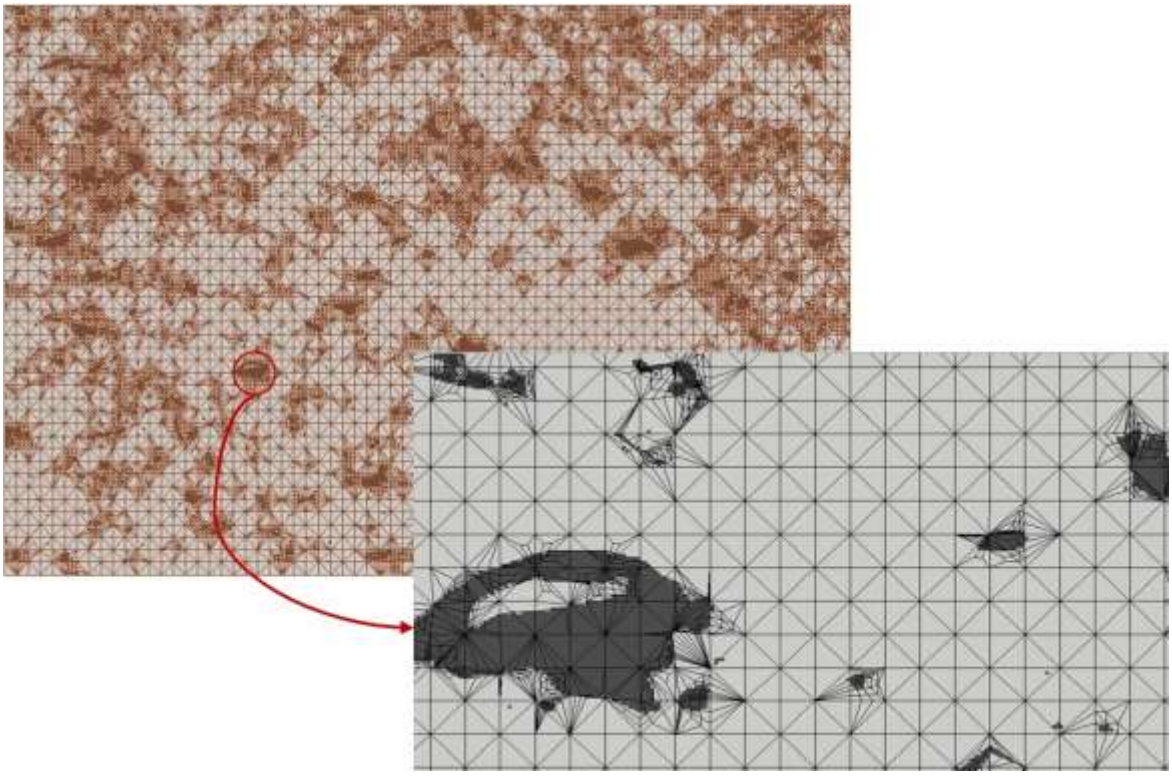

Figure 6. Skeleton and Mesh structure on the micrograph of Al-15Zn coating.

The OOF could solve a Force Balance problem with a defined in-plane displacement. In boundary conditions section, we fixed the left and right sides of the image. A displacement less than the strain at yielding of bulk Al-15Zn should be applied to the boundary of the structure to avoid yielding of the coating. Considering the yield strength and Young's Modulus of pure aluminum, we can derive a yielding strain of 0.002. Therefore, it is safe to apply a displacement of 0.0002 to the right boundary and parallel to the coating plane. The opposing side is set to be fixed, while the top and bottom boundaries are set free. After solving the mesh, the average values of stress and strain in the x-direction over the entire mesh is calculated by OOF. A report from a solved problem, including the average stress and strain from OOF program is shown in Figure 7.

Using the Eq (1), the Young's modulus of the Al-15Az coating could be estimated using object oriented finite element analysis. To achieve a more accurate magnitude of the Young's modulus, this process is repeated for other randomly taken micrographs as well.

$$E = \frac{\sigma_{xx}(1-\nu)}{\varepsilon_{xx}} = 46.7988\,GPa \qquad \text{Eq (1)}$$

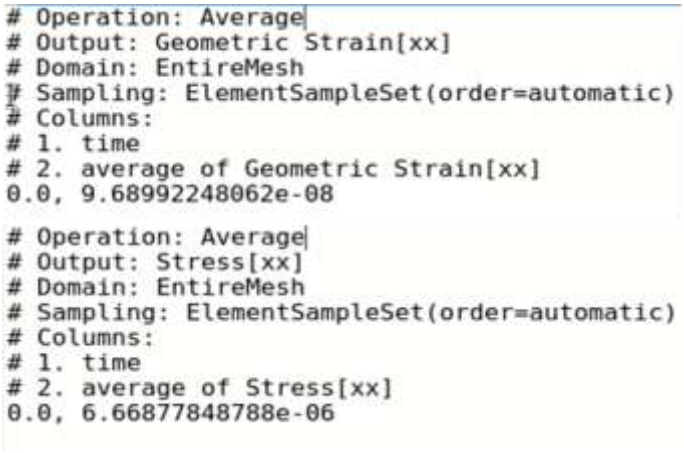

Figure 7. Reported solution by OOF from image analysis of one of the images.

The results show more than 40% reduction in the elastic modulus compared to a bulk of Al-15Zn which is mainly caused by the voids and porosities in the microstructure of the deposited coating. The results are listed in the Table 3.

Table 3. OOF finite element analysis results on two different micrographs.

Group	*Average Strain*	*Average Stress*	*Young's Modulus (GPa)*
Micrograph I	9.6899e-08	6.6687e-06	46.7988
Micrograph II	1.1675e-07	7.5497e-06	43.9713

These results are acceptable according to the available literature and sets a base for us to continue FEA study to better understand the behavior of the coating in service condition where actual experimental test will be a difficult task.

(c) Description of Problems/Challenges

No problems/challenges in this quarter.

(d) Planned Activities for the Next Quarter

The planned activities for next quarter are listed as below:

1) Full-size laboratory tests and data analysis (Task 4.2);
2) Further FEA analysis (image based finite element analysis) and mechanical testing of different coatings (Task 2.5~2.7).

(e) Reference

(1) C. Hsueh, “Effects of Interface Roughness on Residual Stress in Thermal Barrier Coatings”, Journal of American Ceramic society 82, 4, pp. 1073-1075, 1999.

(2) Z. Wang, A. Kulkarni, S. Deshpande, T. Nakamura, and H. Herman, “Effect of Pores and Interface on Effective Properties of Plasma Sprayed Zirconia Coatings“, Acta Materialia, 51, pp. 5319-5334, 2003.